EARLY WATER BREAKTHROUGH IN CARBONATE CORE SAMPLES VISUALIZED WITH X-RAY CT

Toshiya Oshita and Hiroshi Okabe
Japan National Oil Corporation

Abstract

In-situ saturation monitoring during a coreflood with X-ray CT scanner confirmed that the waterflood performance of a mixed-wet, or oil-wet, core plug is totally different from that of a water-wet core plug. Namely, it was observed that brine injected in the mixed-wet, or oil-wet, core plug preferentially invaded into more porous laminae, causing early water breakthrough at an outlet end. This result gives a significant insight into understanding the mechanism of unexpected early water production that has frequently been reported from some giant carbonate reservoirs in the Middle East. Many efforts have been made to grasp how such phenomenon took place. One of the most widely accepted explanations at present ascribes it to reservoir heterogeneities such as the existence of super-permeability streaks. A drawback of this super-permeability concept is, however, that neither cores nor conventional logs can detect such significant variation in permeability that has to be assumed to reproduce the early water breakthrough in a flow simulation model. Thus, in order to provide a better explanation, another factor that also controls the dynamic fluid flow in a reservoir may have to be considered; i.e., wettability. This paper, based upon results of both experimental and numerical studies, aims at associating the wettability distribution in a core sample with the early water breakthrough.

First of all, a couple of coreflood experiments on a single Berea sandstone core plug were conducted under different wettability conditions; i.e., water-wet and mixed-wet. In-situ saturation distribution during each coreflood was monitored with the X-ray CT scanner, which visualized how the early water breakthrough took place within the mixed-wet plug. Then, the similar coreflood experiment was carried out on an oil-wet carbonate core sample taken from a certain reservoir in the Middle East. A numerical simulation study was carried out to reproduce the waterflood performance of each experiment in a computer model and, hence, to investigate the mechanism of the early water breakthrough observed at a core-scale. It was concluded from these studies that the local variation in wettability could exist within the mixed-wet and oil-wet samples. Namely, low porosity laminae are more oil-wet and high porosity laminae are more water-wet, or less oil-wet. As a result, the brine is preferentially imbibed in and runs through the less oil-wet laminae, causing the finger-shaped water encroachment and, finally, the early water breakthrough.

Introduction

Pressure support into many of the gigantic carbonate reservoirs in the Middle East is being achieved by water injection. In order to maximize waterflood recovery efficiency from these reservoirs, the field-wide water encroachment pattern is carefully monitored and every effort is made to control water breakthrough at each of the production wells. In some of them, however, water breakthrough was observed significantly earlier than had originally been predicted (Liu et al., 1993; Webb et al., 1995; Namba et al., 1995). A lot of studies have been conducted to understand how such a phenomenon took place. One of the most likely explanations, which is hence widely accepted by many oil companies at present, ascribes it to reservoir heterogeneities such as the existence of super-permeability (super-k) streaks (Liu et al., 1993). These studies indicate that the field-scale waterflood performance is completely dominated by such super-k streaks although they are very localized within a reservoir. A drawback of this super-k concept is, however, that neither cores nor conventional logs can detect such significant variation in permeability that has to be assumed to reproduce the early water breakthrough in a flow simulation model. As a result, both the existence and distribution of such streaks are often being inferred in some way.

Thus, in order to provide a better explanation, another factor that also controls the dynamic fluid flow in a reservoir may have to be taken into consideration; i.e., wettability. Wettability is defined as the tendency of one fluid to spread on or adhere to a solid surface in the presence of other immiscible fluids (Craig, 1971).

It is well recognized that most clastic reservoir sands are strongly wetted by neither of water and oil phases, and that they tend to be mixed-wet. At a microscopic scale, local wettability on the mineral surface determines the fluid distribution in the crude-oil/brine/rock system. For example, Cryo-SEM work on the mixed-wet Prudhoe Bay cores indicated that aspects of their wettability were closer to dalmatian wettability where there were water-wet and oil-wet regions even in the same pore (Jerauld et al., 1994). NMR analysis on Berea sandstone showed that T_1 distribution shifted to shorter relaxation time for all pore sizes except micropores after aging with a crude oil, qualitatively indicating some regions of the mineral surface were covered with oil films and others with the brine (Zhang et al., 1999). Furthermore, at a core-scale, recent studies have shown that different regions of a given reservoir rock may have different local wetting conditions. In other words, higher permeability laminae may have one type of wettability and lower permeability laminae may have another. Huang et al. (1995) defined these localized wettability conditions as "het-wet," or heterogeneously-wet, and pointed out that the local variation in wettability played an important role in their coreflood experiments on an Aeolian sandstone sample. Introduced in our study is this het-wet concept as a key to understanding the early water breakthrough.

A goal of this paper is, therefore, to associate the wettability distribution within a core sample with the early water breakthrough. First of all, in order to evaluate the effect of wettability alteration on the waterflood performance, a couple of coreflood experiments on a single Berea sandstone core plug were conducted under different wettability conditions; i.e., water-wet and mixed-wet. In-situ saturation distribution during each coreflood was monitored with the X-ray CT scanner, which visualized how (or when and where) the early water breakthrough took place in the mixed-wet case. Then, the same coreflood experiment was carried out on a carbonate core plug acquired from a certain reservoir in the Middle East, of which the wettability was reported to be oil-wet. Applying the het-wet concept to interpretation of the results of these experiments, the mechanism of the early water breakthrough observed at a core-scale was qualitatively investigated using a numerical simulation model.

Experiment

Rock Properties. A Berea sandstone core plug (BD24), with 38 mm in diameter and 70 mm long, was used in the coreflood experiments. This sandstone is mainly composed of quartz with some clay particles such as kaolinite and illite as shown in Figure 1, which is a photograph taken through the scanning electron microscope (SEM). Prior to the coreflooding, porosity of BD24 was measured with our X-ray CT scanner system, which gave the average porosity of 20.2 % and the 3-D porosity distribution as illustrated in Figure 2. Statistical analysis on this CT image indicates that the porosity values range from 15 to 23 %, and that the spatial correlations of the porosity, as measured by variograms, are more than 60 mm along the flow direction (from left to right in Figure 2) and 5 mm across the flow direction. Note there exists in the upper half a lamina with the highest porosity of more than 22 %.

A carbonate rock sample (301B1) used in our study has the same dimensions as the Berea sandstone core plug above. Figure 3 is a thin section image of this carbonate rock. This sample mainly consists of limestone and is classified as bioclastic packstone/grainstone. CT measurement gives the average porosity and its range of 31.8 % and 25 to 40 %, respectively. Figure 4 shows the 3-D porosity distribution of this carbonate core plug. As understood from these two images, pore structure of the carbonate rock is much more complicated than that of Berea sandstone.

Fluid Properties. Refined oil (JS-50) was used as an oil phase, except at an aging stage. Synthetic formation brine was formulated mainly from sodium chloride (NaCl) to give the reservoir salinity. Sodium iodide (NaI) was also added to the brine as a dopant so as to increase an attenuation contrast of X-ray between water and oil phases. Fluid properties used in the coreflood experiments are summarized in Table 1.

Experimental Procedure (1) – for Berea Sandstone. The key steps of the coreflood experiments for the Berea sandstone BD24 are as follows:

1) Take a CT image of the plug under dry condition.
2) Inject brine and take a CT image under 100% brine saturation to calculate the porosity distribution.

3) Inject 100 PV of refined oil to achieve the initial water saturation (S_{wi}) and take a CT image to give the S_{wi} distribution.
4) Displace the refined oil with the brine at a flow rate of 0.05 ml/min until the residual oil saturation (S_{or}) is achieved, with in-situ saturation monitoring by X-ray CT scanning.
5) Inject 100 PV of crude oil, then age the plug at 60°C for 1000 hours.
6) Repeat the steps 3) and 4).

Our previous paper describes a full detail of procedure of the experiment as well as the accuracy of the CT measurements (Oshita et al., 2000). Room temperature was kept at 20°C during the experiment, except the step 5). Both waterfloods were conducted at a low flow rate of 0.05 ml/min. This figure approximately corresponds to a velocity of 1 foot/day, at which a typical water front advances in most reservoirs (Webb et al., 1995). In other words, capillary number of the waterflood in our study is calculated at 10^{-5}; i.e., a capillary pressure dominant process. Fluid permeabilities measured in the course of the above steps are summarized in Table 2.

Experimental Procedure (2) – for Carbonate Rock. Both wettability measurement and coreflooding were carried out on a single core plug (301B1) of the carbonate rock, which had been cleaned with solvents after recovery. The key steps of them are as follows:

1) Take a CT image of the plug under dry condition.
2) Inject brine and take a CT image under 100% brine saturation to calculate the porosity distribution.
3) Inject 100 PV of crude oil, then age the plug at 60°C for 1000 hours.
4) Displace the crude oil with 100 PV of refined oil.
5) Measure spontaneous and forced imbibition of the brine from the S_{wi}.
6) Measure spontaneous and forced imbibition of the refined oil from the S_{or}.
7) Displace the refined oil with the brine at a flow rate of 0.05 ml/min until the S_{or} is achieved.

Forced displacement was chosen, instead of centrifuge, for the wettability measurement because the sample was found to be so friable. Both the wettability measurement and waterflood were conducted at an elevated temperature of 45°C. Other experimental conditions were exactly the same as those for the coreflood on BD24. Fluid permeabilities measured in the course of the above are summarized in Table 2.

Waterflood Performance of Berea Sandstone

Before Aging. In advance of the coreflood experiments on BD24, three more core plugs were cut from the same block of Berea sandstone and their wettability indices were measured by the Amott method at 20°C. These core plugs showed strongly water-wet characteristics. Namely, a large volume of spontaneous imbibition of the brine into the plug from the S_{wi} was observed (I_w = 0.85 – 0.97), while very little oil was imbibed in from the S_{or} without any centrifugal displacement, or forced imbibition (I_o = 0.00 – 0.01). Therefore, the sample BD24 was expected to be strongly water-wet as well.

Figure 5 is a plot of the average water saturation of BD24 as a function of PV of brine injected, which depicts the typical waterflood performance of the strongly water-wet core. Features of the performance are summarized as follows:

- The average S_{wi} was achieved at 18.2 PV%.
- Water breakthrough was observed when 0.32 PV of brine was injected. At the breakthrough, 88 % of recoverable oil had already been produced.
- After the breakthrough, very little further oil production was recorded.
- The S_{or} of 43.6 PV% in average was attained after 10 PV of brine injection.

In-situ saturation monitoring during the waterflood with the X-ray CT scanner provided clear 3-D saturation images within the core plug as displayed in Figure 6(a). It is visually understood from this figure that a Buckley-Leverett type shock front formed as the brine was injected, and that this shock front of brine almost piston-likely displaced the oil.

Aging. After the waterflood under the strongly water-wet condition, the secondary oilflood was carried out with 100 PV of crude oil. The average water saturation at this stage was measured at 15.6 PV%. Then, the

core was aged in a core holder in contact with the crude oil at 60°C for 1000 hours. The crude oil used for aging is classified as Arabian heavy having 28° API gravity, which contains asphaltenes and resins of 6.34 wt% and 3.80 wt%, respectively. During the aging period, the crude oil of at least 1 PV was injected every one week so that a sufficient amount of crude could be in contact with rock surfaces (Webb et al., 1995). Finally, after aging, the crude oil was displaced by the refined oil. This was done so as to prevent the crude oil from remaining in the core plug and, consequently, affecting the subsequent waterflooding or wettability measurements (Graue et al., 1999). The average water saturation after aging was decreased from 15.6 to 8.7 PV%, which was an indication of wettability alteration toward oil-wet side.

After Aging. Four core plugs cut from the same block of Berea sandstone were also aged in the same manner described above. Then, wettability indices were determined by the Amott method at 20°C. All these core plugs showed mixed-wet characteristics. Namely, spontaneous imbibition of both oil and brine was observed; i.e., $I_o = 0.03 - 0.07$ and $I_w = 0.04 - 0.05$. These results are in agreement with those measured on the same sandstone having the same level of initial water saturation by Jadhunandan and Morrow (1995). Therefore, wettability of BD24 was considered to have been altered from strongly water-wet to mixed-wet by aging.

Waterflood on BD24 was conducted under exactly the same experimental conditions as those of the water-wet case, except wettability. Figure 5 also includes a plot of the average water saturation as a function of PV of brine injected in the mixed-wet case. Features of the mixed-wet performance are summarized as follows:

- The average S_{wi} was achieved at 8.7 PV% after aging.
- Earlier water breakthrough was observed when 0.2 PV of brine was injected. At the breakthrough, 65 % of recoverable oil still remained in the core.
- After the breakthrough, continuous oil production was recorded.
- The S_{or} of 29.2 PV% in average was attained after 8.7 PV of brine injection.

Figure 6(b) gives the 3-D saturation images obtained with the X-ray CT scanner. The difference between the water-wet and mixed-wet cases is obvious. Namely, in the waterflooding on the mixed-wet core, no shock front formed at all throughout the process. Instead, injected brine preferentially ran through the most porous lamina that had been detected in the CT derived porosity distribution (Figure 2), causing early water breakthrough. Then, the finger-shaped water encroachment occurred at several porous laminae followed.

Waterflood Performance of Carbonate Rock

The carbonate core plug (301B1) showed strongly oil-wet characteristics at 45°C. Namely, in contrast with the water-wet Berea case, a large volume of spontaneous imbibition of the oil from the S_{or} was observed ($I_o = 0.86$), while very little brine was imbibed in from the S_{wi} without any forced displacement ($I_w = 0.04$).

Figure 7 is a plot of the average water saturation of this carbonate core plug as a function of PV of brine injected. Features of the performance are summarized as follows:

- The average S_{wi} was achieved at 12.4 PV%.
- Very early water breakthrough was observed when only 0.15 PV of brine was injected.
- After the breakthrough, continuous oil production was recorded.
- Ultimate S_{or} seemed not to be attained yet after 15 PV of brine injection, although the average S_{or} reached 41.4 PV% at this stage.

The 3-D saturation images illustrated in Figure 8 reveals the waterflood performance similar to that of the mixed-wet Berea case. Namely, the brine preferentially invaded into the more porous portions within the core plug that could be seen in the CT derived porosity distribution (Figure 4). The water breakthrough was observed, however, much earlier than the mixed-wet BD24. In addition, a route of the water encroachment looks like a tortuous channel, rather than a finger-shape, due to a complicated pore structure.

Numerical Simulation

Model Description. In order to reproduce the waterflood performance and hence investigate the mechanism of the early water breakthrough observed in the mixed-wet Berea sandstone, a numerical simulation model was developed. Total number of voxels to which the CT derived porosity value was assigned is 135252; i.e.,

13 x 102 x 102 (NX x NY x NZ). This data set was averaged into a 2-D model; i.e., 13 x 1 x 51. This averaging was justified by the spatial correlation of porosity along the width of the core. Then, the model was finally expanded in the x-direction (along the length of the core) to 70 x 1 x 51 so as to reduce the numerical dispersion. The absolute permeability in each grid block was determined from a correlation function between permeability and porosity of Berea sandstone (Figure 9), which was derived from our measurement with a probe type porosity-permeability meter. End point saturation data were also obtained from the CT measurements and input to the model. Then, the flow rates, pressure differences across the core, and changes in water saturation were matched to the actual experimental data.

Water-Wet Performance. First of all, the waterflooding on BD24 under the strongly water-wet condition was reproduced in the model. For this, an imbibition capillary pressure curve (Figure 10), measured with our Reservoir Condition Capillary Pressure System, was assigned to all the grid blocks because any local variation in wettability had not been noticed in the water-wet case. In this uniform wettability case, relative permeability was selected as a matching parameter. Then, the waterflood performance was simulated. As revealed in Figure 11, the model satisfactorily reproduced the typical performance of the water-wet core that the shock front of brine almost piston-likely displaced the oil. In Figure 10 are also included the relative permeability curves that gave the best match. These curves are in very good agreement with the representative rock curves of Berea sandstone that were measured in our laboratory (shown by dots in Figure 10), which then ensures the validity of the model.

Mixed-Wet Performance. Using the history matched model above, many case studies were conducted to try to reproduce the finger-shaped water encroachment observed in the mixed-wet case. However, any single capillary pressure curve, or the uniform wettability distribution, could not yield the finger-shape unless extreme contrast of the permeability between the swept and unswept regions was considered; e.g., 1000 md to 10 md. In other words, a super-k streak might have existed within the core plug. It was, however, contradictory to our observations. As shown in Figure 9, measured data of the absolute permeability of Berea sandstone only fell under a range from 100 to 300 md. Thus, it was concluded at this stage that a combination of the uniform wettability and super-k was not enough to explain the mechanism of the finger-shaped water encroachment.

As the next step, therefore, a non-uniform wettability model was built up. Huang et al. (1995) investigated the waterflood performance on a cross-laminated rock slab of Aeolian sandstone before and after aging. They came to a conclusion that the wettability alterations were non-uniform, and that the lower permeability laminae being more oil-wet than the higher permeability ones. The similar situation was noticed in our CT observations. As mentioned earlier, the decrease in the initial water saturation after aging (15.6 to 8.7 PV%) is a sign of wettability alteration toward the oil-wet side, indicating detachment of the water film from the rock surfaces. Figure 12 compares the porosity distribution (a) with the changes in the initial water saturation after aging (b) at a center of BD24. As shown in this figure, the less porous are the laminae, the more decreases the initial water saturation. Figure 12 also shows the in-situ saturation distribution at the water breakthrough (c) at the same location. From these images, it is found that the lower porosity laminae could be more oil-wet, and that the higher porosity laminae could be more water-wet, or less oil-wet, where the brine preferentially invaded during the waterflood.

Based upon the above observation, three sets of imbibition capillary pressure (Figure 13) and relative permeability (Figure 14) were introduced using the empirical model proposed by Saad et al. (1995); i.e., water-wet P_c and k_r, intermediate P_c and k_r, and oil-wet P_c and k_r. Figure 15 shows the best match, among all the runs so far made, to the experimental results on mixed-wet BD24. Although this may not necessarily be a unique solution, changes in both the average water saturation and differential pressure were reasonably reproduced. Figure 16 is a 2-D image of the simulated water saturation distribution at 0.3 PV of brine injection. As demonstrated in this figure, early water breakthrough in the most porous lamina in the upper half of the core plug was successfully reproduced, where the water-wet P_c and k_r curves were assigned. Fingers of water imbibition followed in the porous laminae were also well simulated by the intermediate combination of P_c and k_r. Remaining portions in Figure 16 were assumed to be oil-wet, where the interaction

of oil-wet P_c and k_r delayed the water encroachment.

Note it was only by considering such localized wettability variation that the finger-shaped water encroachment observed during the experiment could be reproduced in the model having a possible and reasonable range of the absolute permeability.

Carbonate Rock. As the finger-shaped, or tortuous-channel-shaped, water encroachment was observed in the waterflood on the carbonate core plug (301B1), the het-wet concept was taken into account also in this case. A numerical simulation model built up is 3-D (55 x 8 x 8), as illustrated in Figure 17, because the sample has the more complicated porosity distribution than Berea sandstone. The absolute permeability was estimated from the hydraulic flow unit (HU) classification of this carbonate reservoir proposed by Abbaszadeh et al. (1996). Then, in the similar way above, three sets of imbibition capillary pressure (Figure 18) and relative permeability (Figure 19) were incorporated into the model. Namely, weakly oil-wet P_c and k_r curves were assigned to the high porosity portion, where the brine was preferentially imbibed at an early stage of the waterflood. Intermediate P_c and k_r curves were used for the surrounding regions of this water conduit, in which the brine invaded next. Remaining portions were considered to be strongly oil-wet, where the interaction of strongly oil-wet P_c and k_r delayed the water encroachment. In this way, as shown in Figure 20, changes in both the average water saturation and differential pressure were reasonably matched to the measured data. Figure 21 is a cross sectional image of the simulated water saturation distribution when 0.2 PV of brine was injected. Finally, as demonstrated in this figure, the early water breakthrough in the more porous portions within the core plug was successfully reproduced in the model. Note, in the carbonate rock case, too, the local variation in wettability, or the het-wet concept, is a key to explain the phenomenon that was observed with the X-ray CT scanner.

Conclusions

The main conclusions in this paper are summarized as follows:

1) As expected, the waterflood performance of a Berea sandstone core sample under the mixed-wet condition was totally different from that under the water-wet condition. This was clearly visualized by in-situ saturation monitoring with the X-ray CT scanner.
2) X-ray CT also visualized the finger-shaped water encroachment during the waterflood of the mixed-wet Berea sandstone core, which occurred at the more porous laminae within the sample. No Buckley-Leverett type shock front was observed at all.
3) The finger-shaped water encroachment of the mixed-wet core was successfully reproduced in a numerical simulation model, where the wettability distribution within the sample (the het-wet concept) must have been taken into consideration in order to explain the observed results. Namely, the low porosity laminae are more oil-wet, while the high porosity laminae more water-wet.
4) Our experimental and numerical studies indicated that although the variation in porosity (and hence permeability) is not so significant within the Berea sandstone core, the local variation in wettability can occur after it has been in contact with the crude oil. As a result, the brine is preferentially imbibed in and runs through the more water-wet laminae, causing the finger-shaped water encroachment and, finally, the early water breakthrough.
5) The finger-shaped, or tortuous-channel-shaped, water encroachment pattern was also observed in the waterflood on the carbonate core plug that showed strongly oil-wet characteristics. The portions through which the brine preferentially invaded are considered to be less oil-wet in the sample. In actual carbonate reservoirs, the similar situation may take place. In such a case, the wettability distribution in a reservoir should be a primary factor that determines a water pass. Namely, not necessarily super-k streaks but higher permeability layers that are frequently encountered in logs can be conduits of the injected water.

Nomenclature

CT	computerized tomography	k_w	water permeability
I_o	Amott wettability index to oil	P_c	capillary pressure
I_w	Amott wettability index to water	PV	pore volume

k_o	oil permeability	S_{wi}	initial water saturation
k_r	relative permeability	S_{or}	residual oil saturation
k_{ro}	relative permeability to oil	μ_o	oil viscosity
k_{rw}	relative permeability to water	μ_w	water (brine) viscosity

Acknowledgement

The authors would like to thank their colleagues in the Reservoir & Recovery Laboratory, Technology Research Center, JNOC for their help and support to this work. The results of this work would not be possible without the dedicated and skilful experimental works by Matsuei Ueki and Hiromi Kaido. Special thanks are also extended to Yasuyuki Mino and Toshiyasu Munakata for their great contribution to establishing our X-ray CT scanner system for advanced core analysis.

References

Abbaszadeh, M., Fujii, H., and Fujimoto, F.: "Permeability Prediction by Hydraulic Flow Units – Theory and Applications," SPE Formation Evaluation (Dec. 1996) 263-271.

Craig, F.F.: "The Reservoir Engineering Aspects of Waterflooding," Monograph Series, SPE, Vol. 3. (1971).

Graue, A., Viksund, B.G., and Baldwin, B.A.: "Reproducible Wettability Alteration of Low-Permeable Outcrop Chalk," SPE Reservoir Eval. & Eng. 2(2) (Apr. 1999) 134-140.

Huang, Y., Ringrose, P.S., and Sorbie K.S.: "The Effects of Heterogeneity and Wettability on Oil Recovery from Laminated Sedimentary Structures," paper SPE 30781 presented at the 1995 SPE Annual Technical Conference and Exhibition, Dallas, U.S.A., Oct. 22-25.

Jadhunandan, P.P., and Morrow, N.R.: "Effect of Wettability on Waterflood Recovery for Crude-Oil/Brine/Rock Systems," SPE Reservoir Engineering (Feb. 1995) 40-46.

Jerauld, G.R., and Rathmell, J.J.: "Wettability and Relative Permeability of Prudhoe Bay: A Case Study in Mixed-Wet Reservoirs," paper SPE 28576 presented at the 1994 SPE Annual Technical Conference and Exhibition, New Orleans, U.S.A., Sep. 25-28.

Liu, J.S. *et al.*: "Integration of Engineering Data and Geostatistics in Simulation of a Complex Carbonate Reservoir," paper SPE 25598 presented at the 1993 SPE Middle East Oil Technical Conference & Exhibition, Bahrain, Apr. 3-6.

Namba, T., and Hiraoka, T.: "Capillary Force Barriers in a Carbonate Reservoir Under Waterflooding," paper SPE 29773 presented at the 1995 SPE Middle East Oil Show, Bahrain, Mar. 11-14.

Oshita, T., Okabe, H., and Namba T.: "Early Water Breakthrough – X-ray CT Visualizes How It Happens in Oil-Wet Cores," paper SPE 59426 presented at the 2000 SPE Asia Pacific Conference on Integrated Modeling for Asset Management, Yokohama, Japan, Apr. 25-26.

Saad, N., Cullick, A.S., and Honarpour, M.M.: "Immiscible Displacement Mechanisms and Scale-Up in the Presence of Small-Scale Heterogeneities," paper SPE 30779 presented at the 1995 SPE Annual Technical Conference and Exhibition, Dallas, U.S.A., Oct. 22-25.

Webb, K.J., Black, C.J.J., and Namba, T.: "Resolving Wettability in a Giant Carbonate Reservoir," paper SPE 36257 presented at the 1996 ADIPEC Conference, Abu Dhabi, U.A.E., Oct. 13-16.

Zhang, G.Q., Huang, C.C., and Hirasaki, G.J.: "Interpretation of Wettability in Sandstones with NMR Analysis," paper SCA-9921 presented at the 1999 International Symposium of the Society of Core Analysts, Golden, Colorado, U.S.A., Aug. 1-4.

	Refined Oil (JS-50)	Brine (NaI + NaCl)
Salinity (ppm)	-	186,000
Density (g/cm^3)		
at 20°C	0.85	1.25
at 45°C	0.83	1.23
at 60°C	0.82	1.22
Viscosity (cp)		
at 20°C	42	2.6
at 45°C	13	1.3
at 60°C	2.3	0.9

Table 1 – Fluid properties.

	Berea Sandstone		Carbonate
	Water-Wet	Mixed-Wet	Rock
S_{wi} (PV%)	18.2	8.7	12.4
1-S_{or} (PV%)	56.4	70.8	58.6
k_w (md)	244	-	6.7
k_o @ S_{wi} (md)	205	181	0.6
k_w @ 1-S_{or} (md)	10	42	0.6

Table 2 – Fluid permeabilities.

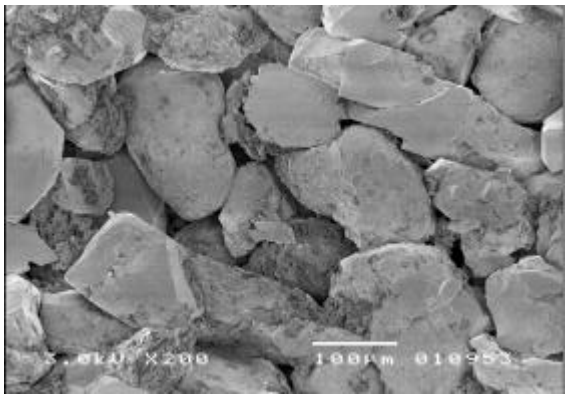

Figure 1 – SEM image of Berea sandstone.

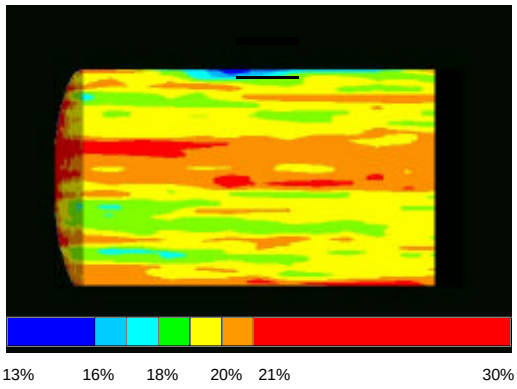

Figure 2 – CT derived 3-D porosity distribution of Berea sandstone (BD24).

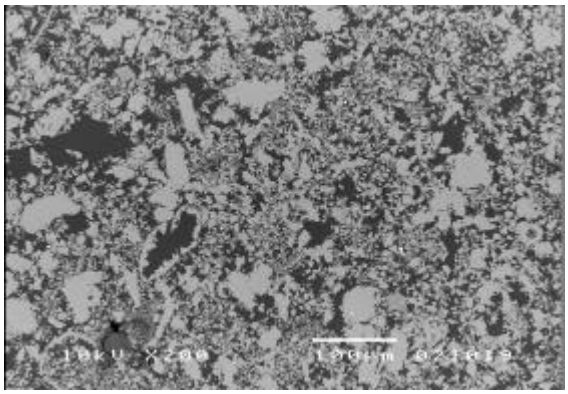

Figure 3 – Thin section image of carbonate rock.

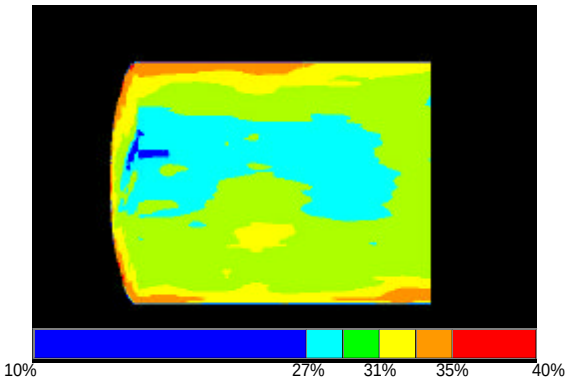

Figure 4 – CT derived 3-D porosity distribution of carbonate rock (301B1).

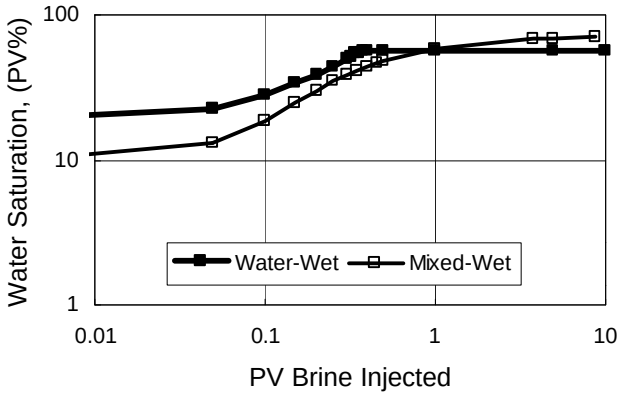

Figure 5 – Average water saturation of Berea sandstone (BD24) as a function of PV of brine injected.

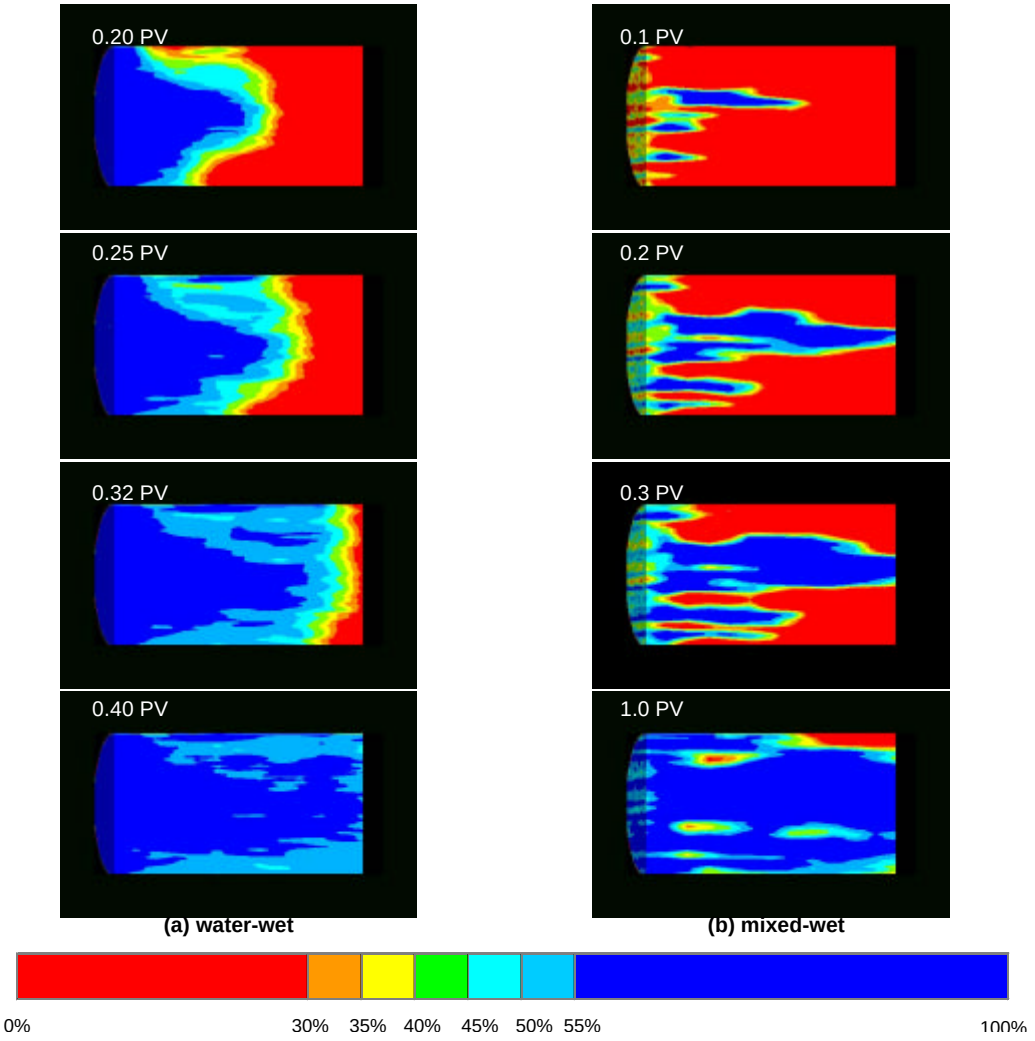

Figure 6 – CT derived water saturation distribution during the waterflood on Berea sandstone (BD24).

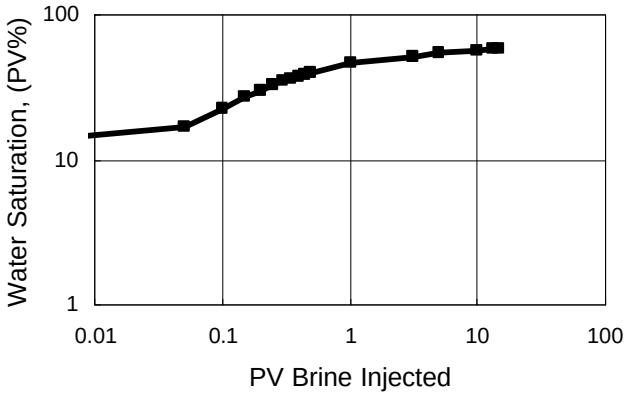

Figure 7 – Average water saturation of carbonate rock (301B1) as a function of PV of brine injected.

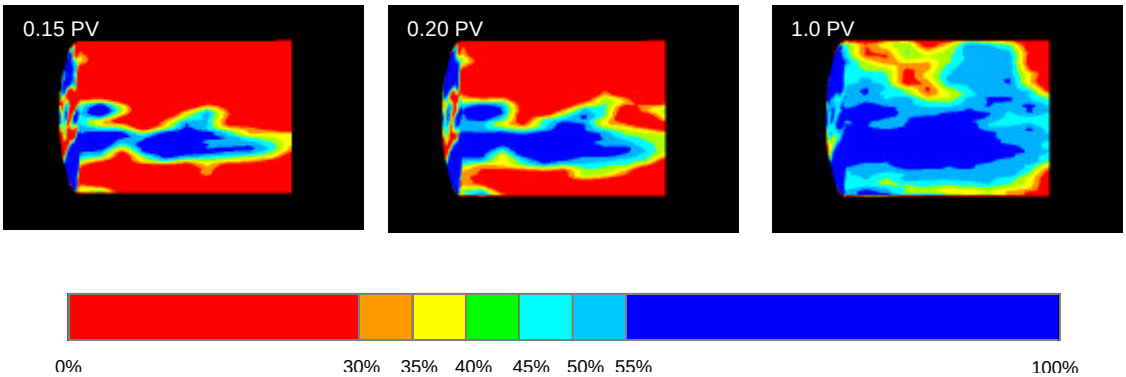

Figure 8 – CT derived water saturation distribution during the waterflood on carbonate rock (301B1).

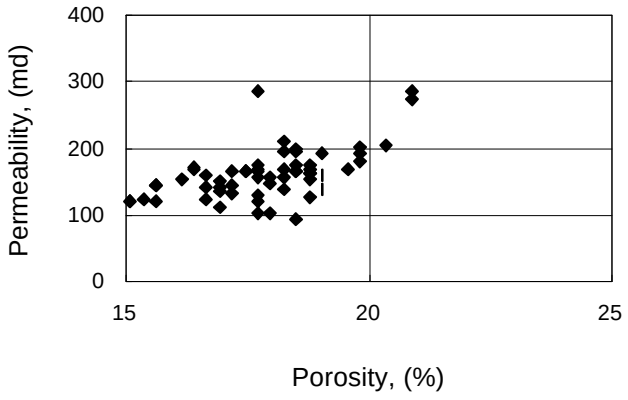

Figure 9 – Permeability – porosity correlation observed on Berea sandstone.

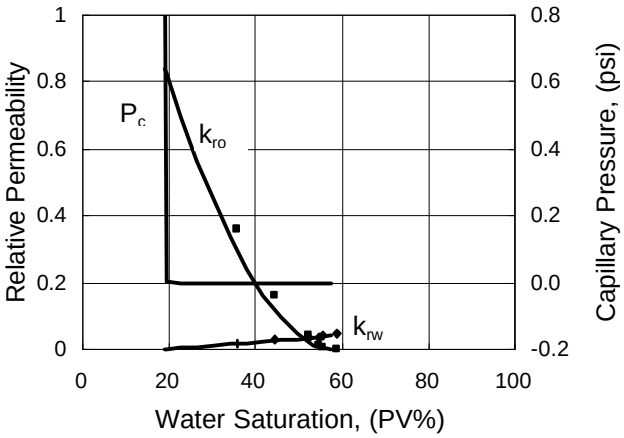

Figure 10 – Imbibition P_c curve in the water-wet model and k_r curves that gave the best match compared to the core data (dots).

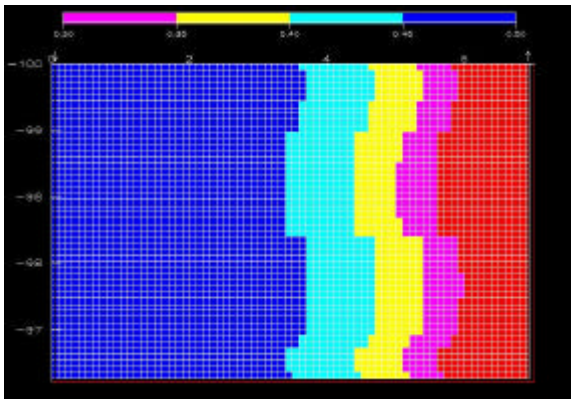

Figure 11 – 2-D image of the simulated water saturation distribution at 0.25 PV of brine injection in the water-wet Berea model.

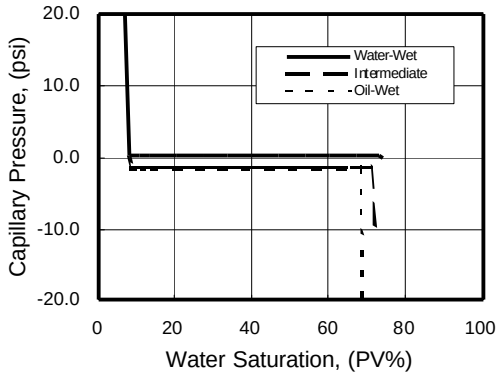

Figure 13 – Three types of imbibition P_c curves in the mixed-wet Berea model.

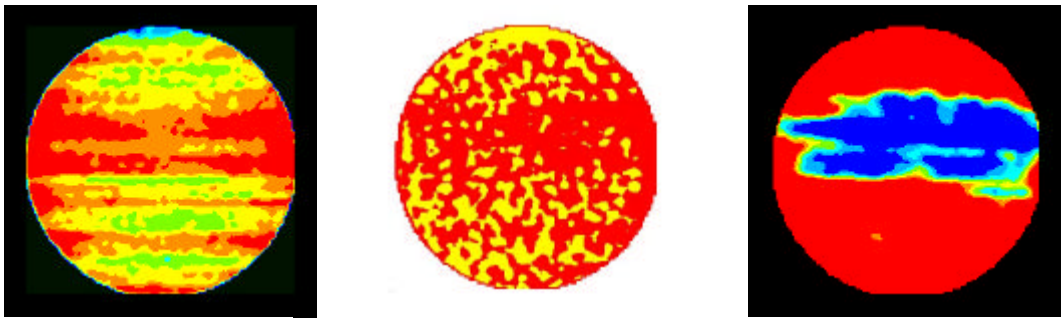

(a) Porosity.

(b) Changes in S_{wi} after aging (yellow: more than 11 PV%).

(c) Water saturation distribution

Figure 12 – CT observations at a center of the Berea sandstone (BD24), indicating the higher porosity laminae, where the brine preferentially invaded during the waterflood, could be more water-wet.

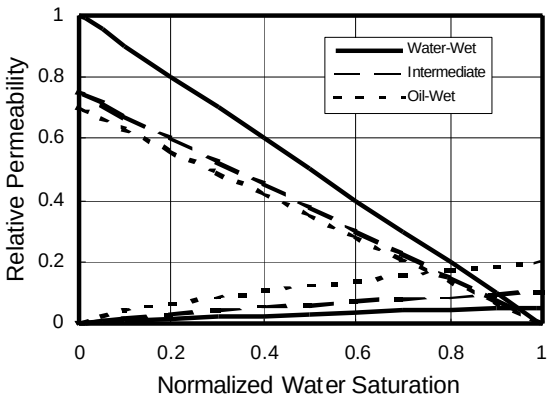

Figure 14 – Three sets of imbibition k_r curves in the mixed-wet Berea model.

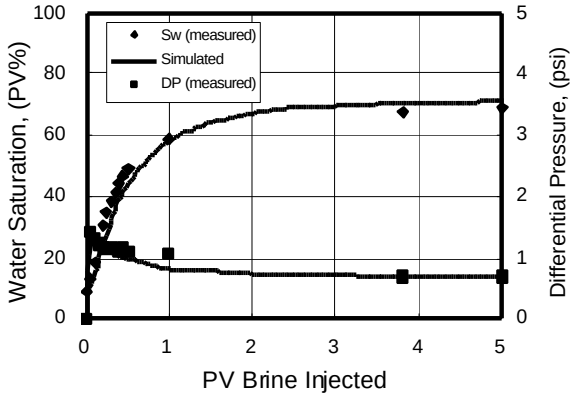

Figure 15 – Measured average water saturation and differential pressure on mixed-wet Berea sandstone (BD24) compared to the simulated results.

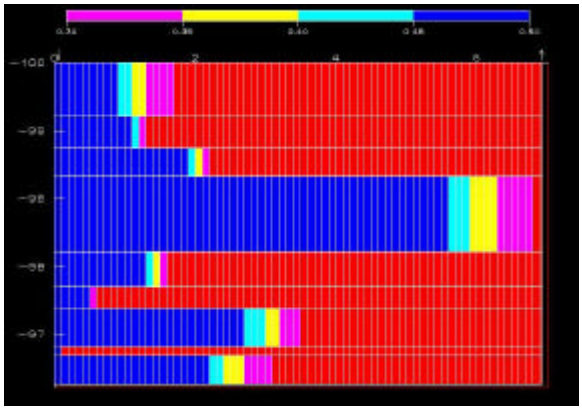

Figure 16 – 2-D image of the simulated water saturation distribution at 0.3 PV of brine injection in the mixed-wet Berea model.

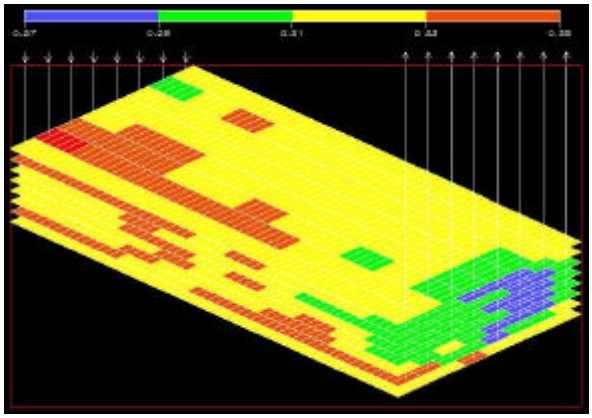

Figure 17 – 3-D model for carbonate rock (301B1).

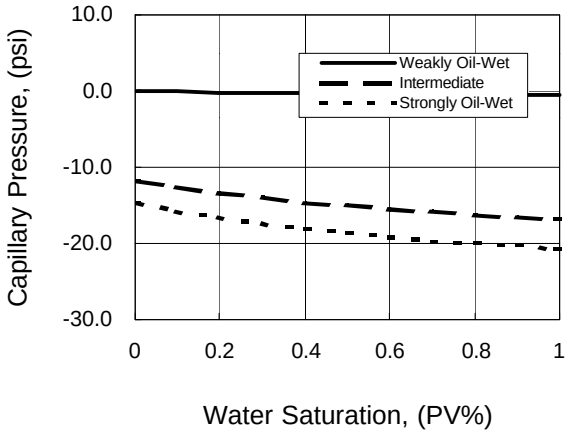

Figure 18 – Three types of imbibition P_c curves in the carbonate rock model.

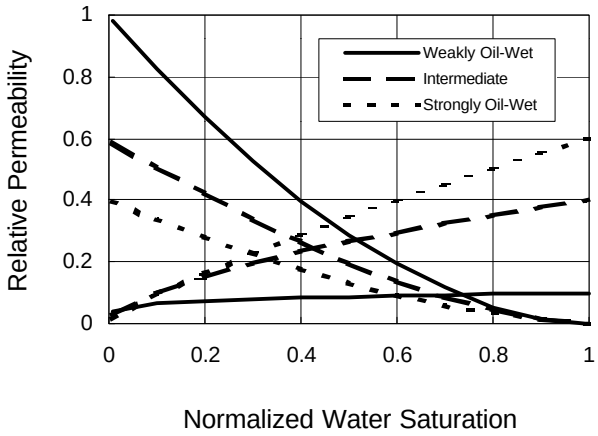

Figure 19 – Three sets of imbibition k_r curves in the carbonate rock model.

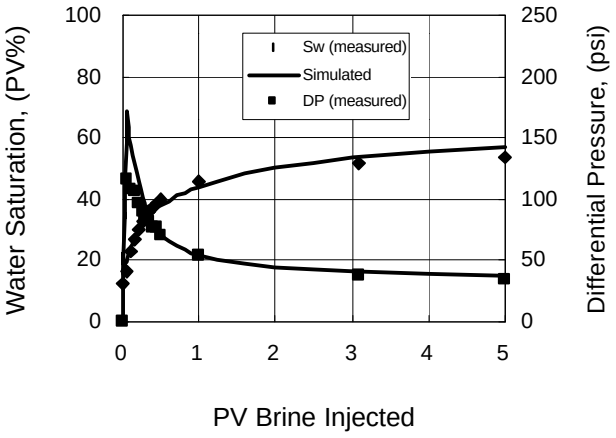

Figure 20 – Measured average water saturation and differential pressure on carbonate rock (301B1) compared to the simulated results.

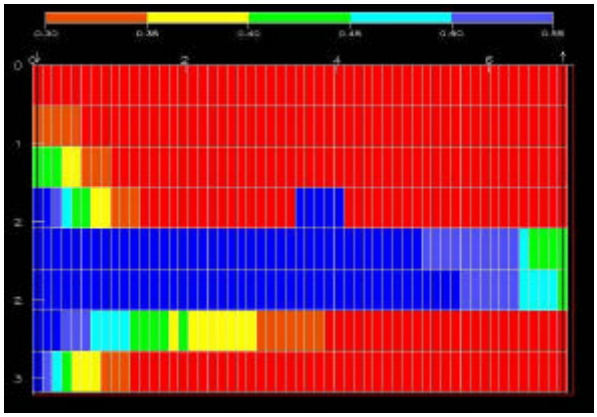

Figure 21 – A cross sectional image of the simulated water saturation distribution at 0.2 PV of brine injection in the carbonate rock model.